

METHODOLOGICAL NOTES

PACS numbers: 41.60 Bq, **41.60. – m,** 78.20.Ci

X-ray Cherenkov radiation near photoabsorption edge

A.P. Potylitsyn, A.V. Vukolov, S.R. Uglov, M.V. Shevelev

DOI: https://doi.org/10.3367/UFNe.2025.05.039926

Contents

1. **Introduction** 1268
2. **Polarization current model** 1269
3. **Vavilov–Cherenkov radiation and transition radiation in 'soft' X-ray range** 1271
4. **Formation length of Vavilov–Cherenkov radiation in absorbing medium** 1272
5. **Angular distribution of Vavilov–Cherenkov X-ray radiation** 1273
6. **Spectral distribution of Vavilov–Cherenkov radiation** 1274
7. **Measurement of Vavilov–Cherenkov radiation spectrum from Be and Si radiators** 1276
8. **Vavilov–Cherenkov radiation in grazing incidence geometry** 1278
9. **Conclusions** 1280

References 1281

Abstract. A radiation mechanism — Vavilov–Cherenkov radiation (VCR) in the soft X-ray region — is considered. A region of anomalous dispersion exists near the photoabsorption edges of some materials where the real part of the permittivity exceeds unity. It is in this narrow frequency range that the VCR mechanism is realized. Analytical expressions for spectral and angular distributions of VCR from a target, an inclined plate, are derived. The VCR formation length is estimated taking into account absorption in the target (radiator) material. An experiment is discussed in which VCR in the 100-eV photon energy range was examined using a 5.7-MeV electron beam from the Tomsk Polytechnic University microtron. Experimental data and theory are shown to be in satisfactory agreement.

Keywords: Vavilov–Cherenkov effect, formation length, anomalous dispersion, X-ray radiation, grazing incidence

1. Introduction

The authors of [1] theoretically and experimentally investigated the radiation characteristics in the frequency range near the L edge of carbon photoabsorption ($\hbar\omega \approx 282$ eV), where the real part of the permittivity becomes positive ($\chi' > 0$) in a very narrow frequency range.

If the real part of the permittivity $\varepsilon(\omega) = 1 + \chi'(\omega) + i\chi''$ in a certain frequency range takes the value $1 + \chi'(\omega) > 1$, the Vavilov–Cherenkov radiation (VCR) mechanism [2, 3] is realized in this frequency range, with photons emitted at the 'Cherenkov' angle $\cos\theta_{ch} = 1/\beta\sqrt{\varepsilon}$. Based on the theory of radiation of a charge passing through a plate of thickness L emitting photons with a frequency ω [4], the authors of the cited work estimated the angle of the Cherenkov cone in the medium as follows:

$$\theta_{ch}^{m} = \sqrt{\chi' - \gamma^{-2}}\,, \tag{1}$$

where γ is the Lorentz factor.

The authors showed that, in this frequency range, radiation absorption in the radiator material is sufficiently high, resulting in the VCR yield being independent of radiator thickness, unlike VCR in the optical range. The spectral distribution of VCR at a fixed radiation angle of $\theta \sim \theta_{ch}^{m}$, which is determined by the energy range $\hbar\omega$ in which the permittivity remains positive, typically does not exceed $\Delta\hbar\omega \sim 1-2$ eV. Thus, the VCR spectrum is a narrow spectral line with a monochromaticity of $\Delta\hbar\omega/\hbar\omega \sim 1\%$.

An additional advantage of the mechanism under consideration is that, as in the optical range of VCR, the radiation characteristics are virtually independent of the Lorentz factor of the charged particle if the charge velocity exceeds the threshold.

A radiation source with similar characteristics based on a compact electron accelerator with an energy of 5–20 MeV is of interest for applied studies. To date, several cycles of experimental studies have been conducted [5–11], the results of which are mainly described in the approach [12] based on the theory of transition radiation [4, 13]. However, some measurements were not adequately described [8, 9, 11], which requires further analysis.

In the approximation of small photon emission angles VCR ($\theta \ll 1$), the expression was used in [5, 6] to estimate the spectral-angular density of VCR

$$\frac{d^2W}{\hbar\, d\omega\, d\Omega} = \frac{\alpha\theta^2}{\pi^2}\left|\frac{1}{\gamma^{-2} - \chi' + \theta^2} - \frac{1}{\gamma^{-2} + \theta^2}\right|^2. \tag{2}$$

Here, θ is the angle between the electron momentum and the wave vector in a vacuum. The resulting expression is only

A.P. Potylitsyn (*), **A.V. Vukolov, S.R. Uglov, M.V. Shevelev**
National Research Tomsk Polytechnic University,
prosp. Lenina 30, 634050 Tomsk, Russian Federation
E-mail: (*) potylitsyn@tpu.ru

Received 22 February 2025, revised 25 April 2025
Uspekhi Fizicheskikh Nauk **195** (12) 1340 – 1355 (2025)
Translated by M.Zh. Shmatikov

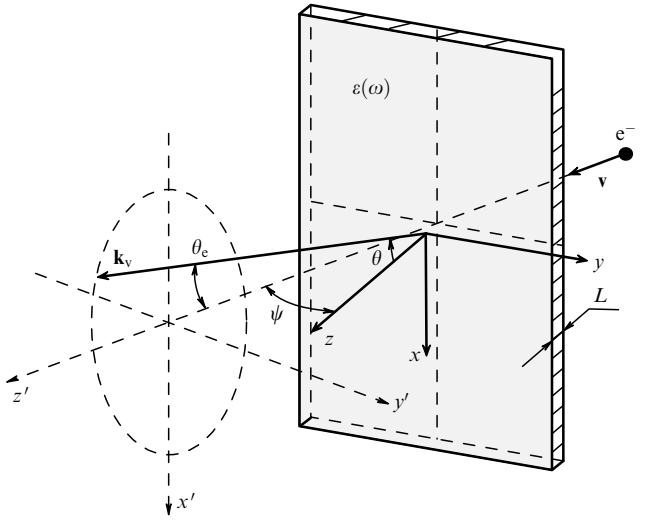

Figure 1. Geometry of VCR process and variables describing process; $\mathbf{k}_\mathrm{v}$ is wave vector of VCR photon in vacuum ($|\mathbf{k}_\mathrm{v}| = \omega/c$).

valid for the perpendicular flight of the charge through the radiator [4]. In spectral measurements with a carbon radiator, the authors of [1] obtained a significant excess of photons with an energy of ~ 280 eV compared to background measurements for an observation angle $\theta = 8.42 \times 10^{-2}$, which is in good agreement with estimate (1). Subsequently, the authors conducted detailed experiments to observe Cherenkov radiation in the soft X-ray range in various radiators [6–10]. Experiments [6–10] were carried out for a perpendicular geometry in the energy range of 100–450 eV using radiators such as carbon, aluminum, silicon, titanium, and vanadium.

Overall, satisfactory agreement was obtained with estimates based on Eqn (2); however, for example, for silicon and carbon radiators, the same value of the Cherenkov angle (1) was obtained in [6], which contradicts the model presented in [1, 5].

The authors of [10] investigated Cherenkov radiation from beryllium and silicon radiators and, after comparing the obtained results with V.E. Pafomov's [13], concluded that the model presented in [13] better agrees with the experiment. The authors of [11, 12] obtained an estimate of the VCR yield for the grazing incidence geometry, which was several times greater than the VCR yield for perpendicular incidence. However, rather crude models were used in [11, 12]. Based on the polarization current model [14–16], we derived a formula for the VCR intensity near the photoabsorption edges, which is valid for an arbitrary geometry (Fig. 1), including the grazing incidence geometry.

2. Polarization current model

V.E. Pafomov developed in [13] a model describing the radiation of a charge passing through a plate of thickness L with permittivity ε at an arbitrary angle. This model takes into account the reflection of the emitted radiation by the input and output surfaces of the plate, which leads to an extremely cumbersome form of the resulting expressions.

In [14–17], the so-called polarization current model (PCM) was developed, in which the radiation of the medium through which the charge passes is considered a 'response' to the excitation of atomic electrons by the charge's electric field [18]. Unlike the cited work by V.E. Pafomov, which considered a plate with infinite transverse dimensions, the PCM allows one to consider radiators of finite size in all three directions.

The Coulomb field of a charge $\mathbf{E}_0$ passing through a radiator of thickness L at a velocity v induces a so-called 'polarization current'

$$\mathbf{j}_\mathrm{pol}(\omega) = \int_{V_\mathrm{R}} \sigma(\omega)\, \mathbf{E}_0(\mathbf{r}, \omega)\, \exp\left(-\mathrm{i}\mathbf{k}\mathbf{r}\right) \mathrm{d}\mathbf{r}\,. \tag{3}$$

Here, $\sigma(\omega) = -\mathrm{i}\omega\,(\varepsilon - 1)/4\pi$, ε is the permittivity of the medium, $|\mathbf{k}| = \sqrt{\varepsilon}(\omega/c)$, and the integration in (3) is carried out over the radiator volume in the coordinate system $\{x, y, z\}$, where the z-axis coincides with the normal to the output surface (see Fig. 1).

For the X-ray range, the transverse dimensions of the radiator greatly exceed the radiation wavelength, allowing the formula for the field $\mathbf{E}_0$, which depends on only one longitudinal coordinate z, to be used in (3) [16, 17].

In this case, the integral over the volume in (3) is reduced to a one-dimensional integral within the limits $\{-L, 0\}$. The known polarization current is used to determine the magnetic field of the radiation in the radiator volume, which is expressed in terms of the wave vector components in the medium:

$$\begin{aligned}
&\mathbf{H}^\mathrm{R}(\omega) = \frac{\exp\left[\mathrm{i}\sqrt{\varepsilon}(\omega/c)r\right]}{r}\,\frac{\mathrm{i}}{c}\,\left[\mathbf{k}, \mathbf{j}_\mathrm{pol}\right],\\
&\mathbf{k} = \frac{\sqrt{\varepsilon}\omega}{c}\,\mathbf{n}_m\,,\\
&\mathbf{n}_\mathrm{m} = \{n_x, n_y, n_z\} = \{\sin\theta_\mathrm{m}\sin\varphi, \sin\theta_\mathrm{m}\cos\varphi, \cos\theta_\mathrm{m}\}\,.
\end{aligned} \tag{4}$$

The magnetic field of the radiation in the medium is described in terms of the angular variables θ_m and φ. After calculations, we obtain

$$\begin{aligned}
\mathbf{H}^\mathrm{R}(\omega) = \frac{e}{2\pi c}\,\frac{\exp\left(\mathrm{i}kr\right)}{r}\,\frac{\beta_z\sqrt{\varepsilon}\,(\varepsilon - 1)}{1 - (\beta_y\sqrt{\varepsilon}\,n_y + \beta_z\sqrt{\varepsilon}\,n_z)}\\
\times\,\frac{\mathbf{H}_0\left\{1 - \exp\left[-\mathrm{i}\,(L\omega/\beta_z c)\,(1 - \beta_y\sqrt{\varepsilon}\,n_y - \beta_z\sqrt{\varepsilon}\,n_z)\right]\right\}}{\beta_z^2\left[\varepsilon(n_x^2 + n_y^2) - 1\right] + (1 - \beta_y\sqrt{\varepsilon}\,n_y)^2},
\end{aligned} \tag{5}$$

where the vector part of the field $\mathbf{H}_0$ is represented as

$$\begin{aligned}
\mathbf{H}_0 = \big\{&\beta_z(\beta_z n_y - \beta_y n_z) - n_y\big(1 - (\beta_y n_y + \beta_z n_z)\sqrt{\varepsilon}\big)\,,\\
&-\beta_z^2 n_x + n_x\big(1 - (\beta_y n_y + \beta_z n_z)\sqrt{\varepsilon}\big), \beta_z\beta_y n_x\big\}\,.
\end{aligned} \tag{6}$$

In Eqns (5) and (6), β_y and β_z denote the components of the charge velocity in units of the speed of light in the coordinate system shown in Fig. 1:

$$\beta_y = \beta\sin\psi;\quad \beta_z = \beta\cos\psi;\quad \beta = \sqrt{1 - \gamma^{-2}}\,.$$

Given the known magnetic field of radiation in the medium $\mathbf{H}^\mathrm{R}$, the electric field $\mathbf{E}^\mathrm{R}$ is found:

$$\mathbf{E}^\mathrm{R} = -\frac{[\mathbf{n}_\mathrm{m}\,\mathbf{H}^\mathrm{R}]}{\sqrt{\varepsilon}}\,. \tag{7}$$

As shown in [17], the electric field of radiation in a vacuum $\mathbf{E}^\mathrm{v}$ is determined by the magnetic field in the medium and the

Fresnel refractive indices F_p, F_s:

$$E_{\parallel}^{\mathrm{v}} = \sqrt{\varepsilon}\, F_p E_{\parallel}^{\mathrm{R}} = F_p\, H_{\perp}^{\mathrm{R}}\,,$$
$$E_{\perp}^{\mathrm{v}} = F_s\, E_{\perp}^{\mathrm{R}} = \frac{F_s H_{\parallel}^{R}}{\sqrt{\varepsilon}}\,, \tag{8}$$

where the field components $E_{\parallel}^{\mathrm{R}}$ and $E_{\perp}^{\mathrm{R}}$ correspond to parallel and perpendicular polarization. In the former case, the polarization plane coincides with the plane passing through the wave vector and the perpendicular to the radiator face through which the radiation is emitted into the vacuum. In the latter case, the polarization plane is perpendicular to this plane.

To find these components, we introduce a unit vector $\mathbf{n}_{\mathrm{v}}$ along the wave vector in the vacuum and polarization unit vectors through the normal to the radiator output surface $\mathbf{b} = \{0, 0, 1\}$:

$$\mathbf{n}_{\mathrm{v}} = \{\mathbf{n}_{\mathrm{v}x}, \mathbf{n}_{\mathrm{v}y}, \mathbf{n}_{\mathrm{v}z}\} = \frac{\{\sin\theta\sin\varphi, \sin\theta\cos\varphi, Z\}}{\sqrt{\varepsilon}}\,,$$
$$Z = \sqrt{\varepsilon - \sin^2\theta}\,,$$
$$\mathbf{e}_1 = \frac{[\mathbf{n}_{\mathrm{v}}, \mathbf{b}]}{\left|[\mathbf{n}_{\mathrm{v}}, \mathbf{b}]\right|} = \{\cos\varphi, -\sin\varphi, 0\}\,,$$
$$\mathbf{e}_2 = [\mathbf{e}_1, \mathbf{n}_{\mathrm{v}}] = \frac{1}{\sqrt{\varepsilon}}\,\{-Z\sin\varphi, -Z\cos\varphi, \sin\theta\}\,. \tag{9}$$

With this choice, the unit vector $\mathbf{e}_1$ is perpendicular to the plane $(\mathbf{n}_{\mathrm{v}}, \mathbf{b})$, and the unit vector $\mathbf{e}_2$ is parallel to it.

Thus, the components $E_{\parallel}^{\mathrm{v}}$, $E_{\perp}^{\mathrm{v}}$ are found from the expression

$$E_{\parallel}^{\mathrm{v}} = F_{\mathrm{p}}(\mathbf{H}^{\mathrm{R}}\mathbf{e}_1), \quad E_{\perp}^{\mathrm{v}} = \frac{F_{\mathrm{s}}(\mathbf{H}^{\mathrm{R}}\mathbf{e}_2)}{\sqrt{\varepsilon}}\,. \tag{10}$$

To describe the radiation field E^{v} in a vacuum, it is necessary to make the replacement $\mathbf{n}_{\mathrm{m}} \to \mathbf{n}_{\mathrm{v}}$ in Eqns (5) and (6), simultaneously expressing the Fresnel coefficients in terms of the vacuum angles θ, φ (i.e., taking Snell's law into account):

$$F_{\mathrm{s}} = 2\,\frac{\cos\theta_{\mathrm{m}}\sin\theta}{\sin(\theta_{\mathrm{m}} + \theta)} = \frac{2Z}{\cos\theta + Z}\,, \tag{11}$$

$$F_{\mathrm{p}} = \frac{\sin 2\theta_{\mathrm{m}}}{\sin(\theta_{\mathrm{m}} + \theta)\cos(\theta_{\mathrm{m}} - \theta)} = \frac{2Z}{\varepsilon\cos\theta + Z}\,. \tag{12}$$

Note that, during refraction, the azimuthal angle does not change ($\varphi_{\mathrm{m}} = \varphi$).

Using the known radiation field, the spectral-angular distribution of the radiation intensity is found:

$$\frac{\mathrm{d}^2 W}{\hbar\,\mathrm{d}\omega\,\mathrm{d}\Omega} = c\left(|E_{\parallel}|^2 + |E_{\perp}|^2\right) = \frac{\alpha}{\pi^2}\, G_0 G_{\mathrm{int}}(G_{\parallel} + G_{\perp}), \tag{13}$$

where

$$G_0 = \frac{\beta_z^2}{\left[(1 - \beta_y n_y)^2 - \beta_z^2\cos^2\theta\right]^2}\left|\frac{\varepsilon - 1}{\varepsilon}\right|^2,$$
$$G_{\mathrm{int}} = \left|\frac{1 - \exp\left[\mathrm{i}L\omega/\beta_z c\,(1 - \beta_z Z - \beta_y n_y)\right]}{1 - \beta_z Z - \beta_y n_y}\right|^2, \tag{14}$$
$$G_{\parallel} = \left|(\beta_z^2 + \beta_y n_y + \beta_z Z - 1)\sin\theta - \beta_y\beta_z\cos\varphi Z\right|^2 \times \left|\frac{Z\varepsilon}{\varepsilon\cos\theta + Z}\right|^2,$$
$$G_{\perp} = |\beta_z\beta_y\sin\varphi\varepsilon|^2\left|\frac{Z}{\cos\theta + Z}\right|^2.$$

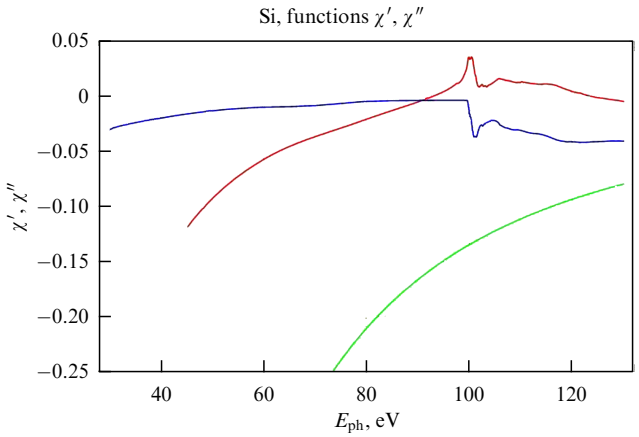

Figure 2. Functions χ' and χ'' characterizing permittivity of silicon (red and blue curves) and dependence $\chi'(\omega) - 1 = -\omega_{\mathrm{p}}^2/\omega^2$ (green curve).

Equations (13) and (14) describe radiation in the 'forward' direction, i.e., into the forward hemisphere. Expression (13) was successfully used in [19] to describe the spectrum of optical Cherenkov radiation in a frequency-dispersive radiator (quartz).

It should be noted that, in the PCM, Cherenkov radiation and transition radiation (TR) are considered manifestations of a single mechanism for excitation of the medium, i.e., they are different types of polarized radiation [14]. Thus, Eqn (13) describes both VCR and TR for the corresponding geometry. In the latter case, using Eqn (13), we obtain the characteristics of the so-called forward transition radiation.

Below, we consider X-ray VCR near the L edge of silicon ($\hbar\omega \leqslant 100$ eV), where the permittivity is represented as [20]

$$\varepsilon(\omega) = z_1 + \mathrm{i}z_2 = 1 - \frac{\omega_p^2}{z_{\mathrm{Si}}\omega^2}\,(f_1 + \mathrm{i}f_2)$$
$$= 1 + \chi' + \mathrm{i}\chi'', \quad |\chi'|,\ |\chi''| \ll 1\,. \tag{15}$$

Figure 2 shows the dependences $\chi'(\omega)$, $\chi''(\omega)$ in the range $40 < \hbar\omega < 120$ eV. For comparison, the same figure displays the dependence $\varepsilon(\omega) = 1 - \omega_p^2/\omega^2$ ($\omega_p = 32$ eV), which is widely used to calculate TR characteristics in the harder X-ray range ($\omega > 5$ keV) [13]. For silicon, $z_{\mathrm{Si}} = 14$, $\omega_p = 32$ eV; the functions f_1, f_2 are tabulated in [20].

We now consider the main characteristics of the interference function G_{int}. After a series of algebraic calculations, a simpler and more intuitive expression can be obtained for the interference function G_{int}:

$$G_{\mathrm{int}} = \frac{1 - 2\cos p\exp(q) + \exp(2q)}{p_0^2 + q_0^2}\,,$$
$$p_0 = 1 - \beta_y n_y - \beta_z\mathrm{Re}\left(Z(\omega)\right) = 1 - \beta_y n_y - \beta_z \times \left[\frac{1}{2}\left(z_1 - \sin^2\theta + \sqrt{(z_1 - \sin^2\theta)^2 + z_2^2}\right)\right]^{1/2},$$
$$q_0 = -\beta_z\,\mathrm{Im}\left(Z(\omega)\right) = -\beta_z\left[\frac{1}{2}\left(\sqrt{(z_1 - \sin^2\theta)^2 + z_2^2} - (z_1 - \sin^2\theta)\right)\right]^{1/2},$$
$$p = \frac{L\omega}{\beta_z c}\,p_0 = \frac{2\pi L}{\beta_z\lambda}\,p_0\,, \tag{16}$$
$$q = \frac{L\omega}{\beta_z c}\,q_0 = \frac{2\pi L}{\beta_z\lambda}\,q_0\,.$$

In (16), λ is the radiation wavelength.

The dependence of the function $G_{\rm int}$ on the radiator thickness L is determined by the quantities p, q.

Disregarding radiation absorption in the radiator material ($q_0 \to 0$), the condition $p_0 = 0$ yields the formula for the 'Cherenkov' angle $\theta_{\rm ch}$ in a vacuum (see Fig. 1):

$$1 - \beta \sin\psi \sin\theta_{\rm ch} - \beta \cos\psi \sqrt{\varepsilon - \sin^2\theta_{\rm ch}} = 0\,, \qquad (17)$$

if $\varphi = 0$.

In this approximation, from (16) we obtain

$$G_{\rm int,\,0} = \frac{2\,(1-\cos p)}{p_0^2} = \frac{4\sin^2(p/2)}{p_0^2} = 4\left(\frac{\pi L}{\beta_z \lambda}\right)^2 \frac{\sin^2(p/2)}{(p/2)^2}\,. \qquad (18)$$

Next, we consider the geometry of the perpendicular flight of an ultrarelativistic electron through a radiator, taking absorption into account ($\gamma \gg 1$, $\psi = 0$, $\beta_y = 0$, $\beta_z = \beta$). In the small-angle approximation ($\theta^2 \sim \chi' < 1$), we obtain the following formula:

$$p_0 = 1 - \beta\sqrt{1 + \chi' - \theta^2 + \frac{\chi''^2}{4}} = \frac{1}{2}\left(\chi' - \gamma^{-2} - \theta^2 + \frac{\chi''^2}{4}\right),$$
$$q_0 = \frac{\chi''}{2}\,.$$

From the condition $p_0 = 0$, we obtain an expression for the angle $\theta_{\rm ch}$ (for $\chi''^2 \ll \chi'$):

$$\theta_{\rm ch} = \sqrt{\chi' - \gamma^{-2}}\,,$$

which coincides with the result obtained in [1].

In an absorbing medium, the formula for the Cherenkov angle $\theta_{\rm ch}^{\rm m}$ was derived in [21, 22] based on the expression for energy losses:

$$\cos^2\theta_{\rm ch}^{\rm m} = \frac{{\rm Re}\,\varepsilon}{\beta^2 |\varepsilon|^2}\,. \qquad (19)$$

In the X-ray range, we obtain from (19) an estimate accurate to terms of second-order smallness:

$$\cos^2\theta_{\rm ch}^{\rm m} = \frac{1+\chi'}{(1-\gamma^{-2})\left[(1+\chi')^2 + \chi''^2\right]} \approx 1 + \gamma^{-2} - \chi'\,. \qquad (20)$$

For angles $\theta_{\rm ch}^{\rm m} \ll 1$, this implies the relation

$$(\theta_{\rm ch}^{\rm m})^2 \approx \chi' - \gamma^{-2}\,.$$

The result obtained coincides with Eqn (1), which is not surprising, since, due to the smallness of the refractive index $\sqrt{1+\chi'}$, the angular distribution of the VCR in a vacuum is broadened by a second-order smallness. Thus, in the approximation used, $\theta_{\rm ch}^{\rm m} \approx \theta_{\rm ch}$.

Ignoring the absorption of radiation in the radiator material ($q_0 = 0$), which is approximately true in the optical range, instead of Eqn (16), we have the formula (for $p \to 0$)

$$G_{\rm int,\,0} = 4\left(\frac{\pi L}{\beta\lambda}\right)^2 \frac{\sin^2(p/2)}{p^2/4} = 4\left(\frac{\pi L}{\beta\lambda}\right)^2. \qquad (21)$$

The quadratic dependence of the VCR intensity on the radiator thickness transforms into a standard linear dependence after integration over the angular variables. In the range under study ($\hbar\omega \leqslant 1$ keV), strong absorption of radiation, characterized by the parameter q, results in the function $G_{\rm int}$ being independent of the thickness L. Indeed, it is easy to derive a simple formula accurate to second-order terms:

$$q \approx -\frac{\pi L \chi''}{\lambda} = -\frac{L}{2\ell_{\rm abs}}\,, \qquad (22)$$

where $\ell_{\rm abs} = \lambda/2\pi\chi''$ is the absorption length [11].

For radiator thicknesses $L > 5$ μm, $|q| \gg 1$, and therefore, for $\exp(q) = \exp(-L/2\ell_{\rm abs}) \ll 1$, we have

$$G_{\rm int} = \frac{1}{p_0^2 + q_0^2} = \frac{4}{(\chi' - \gamma^{-2} - \theta^2)^2 + \chi''^2}\,,$$

and, consequently,

$$\frac{{\rm d}^2 W}{\hbar\,{\rm d}\omega\,{\rm d}\Omega} = \frac{\alpha\theta^2}{\pi^2} \frac{\chi'^2 + \chi''^2}{(\gamma^{-2} + \theta^2)^2\left[(\gamma^{-2} + \theta^2 - \chi')^2 + \chi''^2\right]}\,. \qquad (23)$$

The resulting expression. which coincides with Eqn (2.85) in [1], is more accurate than formula (2).

For transition radiation in the harder range ($\hbar\omega > 5$ keV), where absorption is significantly lower, from Eqn (16) we obtain

$$\begin{aligned} G_{\rm int} &= \frac{\left(1 - \exp(q)\right)^2 + 4\sin^2(p/2)\exp(q)}{p_0^2 + q_0^2} \\ &= 4\left\{\left[1 - \exp\left(-\frac{L}{2\ell_{\rm abs}}\right)\right] \right. \\ &+ 4\sin^2\left[\frac{\pi L}{2\lambda}\left(\frac{\omega_{\rm p}^2}{\omega^2} + \gamma^{-2} + \theta^2\right)\right] \\ &\times \left.\exp\left(-\frac{L}{2\ell_{\rm abs}}\right)\right\} \times \left\{\left(\frac{\omega_{\rm p}^2}{\omega^2} + \gamma^{-2} + \theta^2\right)^2 \right. \\ &+ \left.\left(\frac{\lambda}{\pi\ell_{\rm abs}}\right)^2\right\}^{-1}. \end{aligned} \qquad (24)$$

Here, the standard dependence for the hard X-ray range $\chi' = -\omega_{\rm p}^2/\omega^2$ is used. The numerator is completely identical to the result obtained by G.M. Garibyan for transition radiation in [4].

3. Vavilov–Cherenkov radiation and transition radiation in 'soft' X-ray range

For perpendicular geometry, Eqn (23) describes both VCR and transition radiation in the $\hbar\omega \leqslant 1$ keV range. When the Cherenkov condition (1) is satisfied, i.e., under the condition $\theta^2 = \chi' - \gamma^{-2}$, expression (23) reduces to

$$\frac{{\rm d}^2 W}{\hbar\,{\rm d}\omega\,{\rm d}\Omega} = \frac{\alpha}{\pi^2} \frac{(\chi' - \gamma^{-2})(\chi'^2 + \chi''^2)}{\chi'^2\,\chi''^2}\,. \qquad (25)$$

Since $\gamma^{-2} < \chi'$, the radiation intensity at the maximum (25) smoothly increases from a minimum at the threshold Lorentz factor to a maximum at $\gamma^{-2} \ll \chi'$. For the threshold Lorentz factor value $\gamma^{-2} = \chi'$, the Cherenkov radiation

mechanism is not operative, and the radiation characteristics are described by the transition radiation mechanism, for which the maximum radiation intensity is attained at an angle $\theta = \gamma^{-1}$. In this case, from Eqn (23), we have ($\theta^2 = \gamma^{-2} = \chi'$)

$$\frac{\mathrm{d}^2 W}{\hbar\,\mathrm{d}\omega\,\mathrm{d}\Omega} = \frac{\alpha}{\pi^2}\,\frac{1}{4\chi'(\chi'^2 + \chi''^2)}\,. \tag{26}$$

Similar to Cherenkov radiation, for the moderately relativistic case under consideration ($\gamma < 10$), the TR does not depend on the Lorentz factor.

In the ultrarelativistic case, the VCR intensity reaches a maximum at $\theta = \sqrt{\chi'}$:

$$\frac{\mathrm{d}^2 W_{\max}}{\hbar\,\mathrm{d}\omega\,\mathrm{d}\Omega} = \frac{\alpha}{\pi^2}\,\frac{\chi'^2 + \chi''^2}{\chi'\chi''^2}\,. \tag{27}$$

In this case, in the angular range $\theta \sim \gamma^{-1}$, the radiation intensity depends quadratically on the Lorentz factor and is determined by the standard TR mechanism [23]:

$$\frac{\mathrm{d}^2 W}{\hbar\,\mathrm{d}\omega\,\mathrm{d}\Omega} = \frac{\alpha}{\pi^2}\,\frac{\gamma^2}{4\,(\chi'^2 + \chi''^2)}\,.$$

Figure 3a shows the angular distribution of the X-ray VCR intensity for electrons with Lorentz factors $\gamma = 10$, 20, and 150 during perpendicular flight through a 10-μm-thick silicon radiator, calculated using Eqn (18), in comparison with the small-angle approximation (see formula (23)). Over the entire range of γ, the difference does not exceed 5%. Note that the TR intensity of ultrarelativistic electrons in the angular range $\theta \sim \gamma^{-1}$ significantly exceeds the VCR intensity, while the opposite situation is observed for moderately relativistic electrons ($\gamma \leqslant 20$). Similar dependences for the energy $\hbar\omega = 130$ eV, i.e., in the absence of the Cherenkov mechanism, are presented in Fig. 3b.

For comparison, the angular distribution of the TR intensity for $\gamma = 10$ is multiplied by $(\gamma_1/\gamma_2)^2 = (150/10)^2 = 225$.

As expected, the maximum intensity corresponds to the angle $\theta = \gamma^{-1}$. In the ultrarelativistic case ($\gamma = 150$), the PCM and the small-angle approximation yield identical results to within $\sim 10^{-3}$. For $\gamma = 10$, a 5% difference persists. Similar to the standard TR, a dependence close to γ^2 is observed.

4. Formation length of Vavilov–Cherenkov radiation in absorbing medium

Several definitions of the formation length of radiation by a moving charge are available [24–26].

It appears that the definition of the formation length (formation path, coherence length) as the distance at which the charge lags behind the wave front by a wavelength has a clear physical meaning [25, 26] (in contrast to B.M. Bolotovsky's definition [24], which yields a value half as large). This definition is used below.

In the same study, Bolotovsky suggested another definition: "...the formation path is the distance that a particle must travel after the radiation process for its interference with the radiation field to cease" (see p. 100 in [24]). This requirement is precisely fulfilled when determining the formation length in a medium using Eqn (28):

$$L_\mathrm{f} = \frac{\lambda}{1/\beta - \sqrt{\varepsilon}\,\cos\theta}\,. \tag{28}$$

Apparently, in such a medium, the VCR formation length tends to infinity ($\cos\theta = 1/\beta\sqrt{\varepsilon}$). In the case of an absorbing medium ($\varepsilon = z_1 + \mathrm{i}z_2$), V.M. Grishin proposes using the complex formation length (see Eqn (25) in [22]),

$$Z^\mathrm{G}(\omega,\theta) = \frac{\pi\beta c}{\omega}\,\frac{1}{1 - \beta\sqrt{\varepsilon}\cos\theta}\,, \tag{29}$$

which leads to the formula

$$L_\mathrm{f}^\mathrm{G} = \mathrm{Re}\,Z^\mathrm{G}(\omega,\theta)\,.$$

Note that Eqn (29) was derived based on Bolotovsky's criterion [24], so the more common criterion of M.L. Ter-Mikaelyan [25] is used below.

In this case,

$$L_\mathrm{f}^\mathrm{G} = \mathrm{Re}\left|\frac{2\pi\beta c}{\omega}\,\frac{1}{1 - \beta\sqrt{\varepsilon}\cos\theta}\right| = \frac{\beta\lambda}{\mathrm{Re}\,|1 - \beta\sqrt{\varepsilon}\cos\theta|}\,. \tag{30}$$

If we take the value from Eqn (12) in the cited article as the angle $\theta_\mathrm{ch}^\mathrm{m}$,

$$\cos^2\theta_\mathrm{ch}^\mathrm{m} = \frac{\mathrm{Re}\,\varepsilon}{\beta^2|\varepsilon|^2}\,, \tag{31}$$

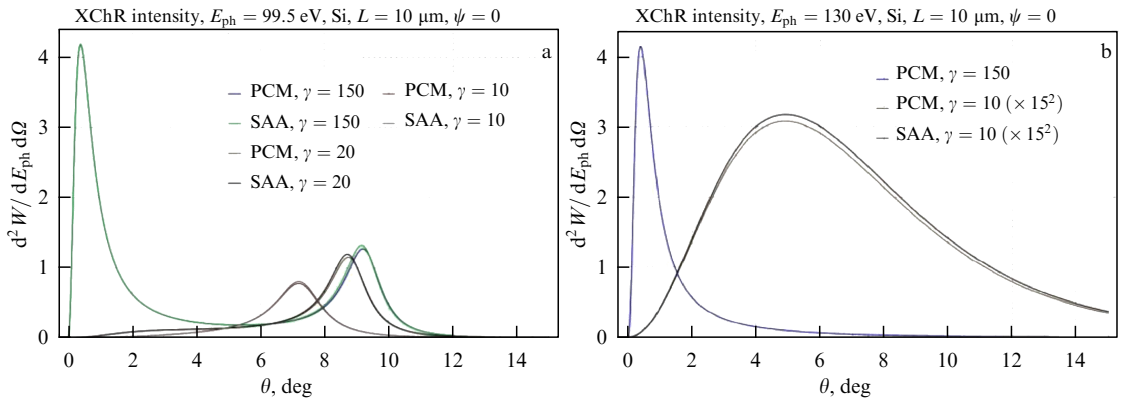

Figure 3. Angular distribution of intensity of radiation of electrons with various Lorentz factors during perpendicular flight through 10-μm-thick silicon plate (PCM is polarization current model, SAA is small-angle approximation): (a) $\hbar\omega = 99.5$ eV — VCR, (b) $\hbar\omega = 130$ eV — TR.

after standard transformations we obtain the following expression:

$$L_{\rm f}^{\rm G} = \frac{\beta\lambda}{1 - \sqrt{\dfrac{1}{2}\left[\dfrac{z_1^2}{z_1^2+z_2^2} + \dfrac{z_1}{\sqrt{z_1^2+z_2^2}}\right]}}\,. \tag{32}$$

Usually, in transparent media, the following relation is satisfied,

$$\frac{z_2^2}{z_1^2} \ll 1\,, \tag{33}$$

which allows us to ignore the following orders of smallness in the expansion of the last expression:

$$L_{\rm f}^{\rm G} \approx \frac{\lambda}{(3/8)\, z_2^2/z_1^2} = \frac{8}{3}\frac{z_1^2}{z_2^2}\,\lambda\,. \tag{34}$$

For the X-ray range under consideration, the formation length found significantly exceeds the absorption length,

$$L_{\rm f}^{\rm G} \approx \frac{8}{3}\frac{\lambda}{\chi''^2} \gg \frac{\lambda}{2\pi\chi''}\,, \tag{35}$$

which is certainly an overestimate.

If we determine the formation length based on the following formula,

$$L_{\rm f} = \frac{\beta\lambda}{|1 - \beta\sqrt{\varepsilon}\cos\theta|}\,, \tag{36}$$

where the 'Cherenkov' angle $\theta_{\rm ch}^{\rm m}$ is determined by the condition that the denominator (i.e., $L_{\rm f} \to \infty$) be zero,

$$\mathrm{Re}\,|1 - \beta\sqrt{\varepsilon}\cos\theta_{\rm ch}^{\rm m}| = 0\,, \tag{37}$$

then, as is shown below, the formation length exceeds the absorption length, but is commensurable to it.

From (37), we obtain the formula for the Cherenkov angle in an absorbing medium:

$$\cos\theta_{\rm ch}^{\rm m} = \frac{1}{\beta\sqrt{1/2\left(z_1 + \sqrt{z_1^2+z_2^2}\right)}}\,. \tag{38}$$

When condition (33) is satisfied, the formula obtained reduces to

$$\cos\theta_{\rm ch}^{\rm m} = \frac{1}{\beta\sqrt{z_1}}\left(1 - \frac{z_2^2}{8z_1^2}\right). \tag{39}$$

In the same approximation, the following formula follows from (31),

$$\cos\theta_{\rm ch}^{\rm mG} \approx \frac{1}{\beta\sqrt{z_1}}\left(1 - \frac{z_2^2}{2z_1^2}\right), \tag{40}$$

which is quite close to the previous one, but yields slightly smaller values.

Substituting Eqn (40) into formula (36), taking into account relation (37), we obtain (provided condition (33) is satisfied)

$$L_{\rm f} = \frac{\lambda}{z_2}\sqrt{2z_1^2 + 2z_1\sqrt{z_1^2+z_2^2} + z_2^2} \approx 2\lambda\,\frac{z_1}{z_2}\left(1 + \frac{z_2^2}{4z_1^2}\right). \tag{41}$$

In our case, $z_1 = 1 + \chi'$, $z_2 = \chi''$, $\chi', \chi'' \ll 1$, so, from Eqn (41), ignoring, as before, the quadratic and higher terms, a simple expression follows:

$$L_{\rm f} = 2\,\frac{\lambda}{\chi''}\,. \tag{42}$$

The obtained result appears more 'physical' since, like the absorption length, it is determined by the quantity λ/χ'', whereas V.M. Grishin's estimate (35) yields a dependence λ/χ''^2 that is more than an order of magnitude greater than the absorption length.

5. Angular distribution of Vavilov–Cherenkov X-ray radiation

The polarization current model allows us to calculate the radiation characteristics for any target (radiator) orientation. For the geometry of an oblique electron flight, we write an equation that follows from the general expression for the Cherenkov pole $p_0 = 0$:

$$1 - \beta\sin\psi\sin\theta\cos\varphi = \beta\cos\psi\,\mathrm{Re}\left(Z(\omega)\right). \tag{43}$$

After squaring both sides of Eqn (43) (here, the geometry $\varphi = 0$ is considered) and disregarding the value $(\chi'')^2$, we obtain a quadratic equation for $\sin\theta_{\rm ch}$, the two solutions of which are represented as

$$\sin\theta_{\rm ch\,1,2} \approx \frac{\sin\psi}{\beta} \pm \cos\psi\,\theta_{\rm ch}^0 \approx \sin\left(\psi \pm \theta_{\rm ch}^0\right). \tag{44}$$

For tilt angles $\psi > \theta_{\rm ch}^0$, the angular dependence of the VCR photon yield on the polar angle θ exhibits two maxima, corresponding to the observation of VCR along the cone generators located on either side of the electron momentum direction in the $\varphi = 0$ plane.

Figure 4a shows the angular distribution of the VCR intensity for a radiator tilt angle of $\psi = 30°$, and Fig. 4b, for $\psi = 60°$. A zero minimum is observed along the electron momentum direction ($\theta = \psi$).

The VCR yield is characterized by two maxima, the locations of which are fairly well described by formula (26) for an angle of $\psi = 30°$, whereas, for an angle of $\psi = 60°$, the disagreement increases. In the latter case, for $\hbar\omega = 99.5$ eV, using Eqn (18), we have $\theta_1^{\rm m} = 31.8°$, $\theta_2^{\rm m} = 49.6°$ (Fig. 4b), while $\theta_{\rm ch}^0 = 8.9°$. For a photon energy of $\hbar\omega = 99.8$ eV, this disagreement reaches 10% ($|\theta_{1,2}^{\rm m} - (\arcsin(\psi \pm \theta_{\rm ch}^0))| \sim 1°$).

It should be noted that, with an increase in the tilt angle ψ, the VCR intensity at the maxima increases. The same figures show the calculated TR dependences for an energy of $\hbar\omega = 130$ eV — typical TR dependences [23].

The angular 'width' of the VCR cone in the case under consideration is determined by $\theta_{\rm ch}^0$ and does not depend on the radiator thickness, in contrast to the optical range, where this parameter is estimated as [3]

$$\Delta\theta \approx \frac{2\lambda}{\pi L\sin\theta_{\rm ch}}\,. \tag{45}$$

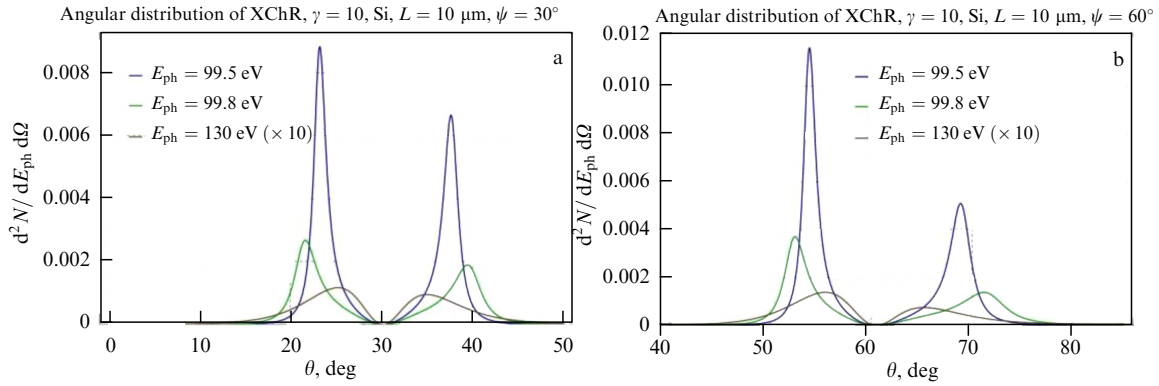

Figure 4. Angular distribution of electron emission with $\gamma = 20$ crossing inclined silicon target 10 μm thick. (a) Inclination angle $\psi = 30°$, (b) $\psi = 60°$. Blue and green colors — VCR, brown — TR.

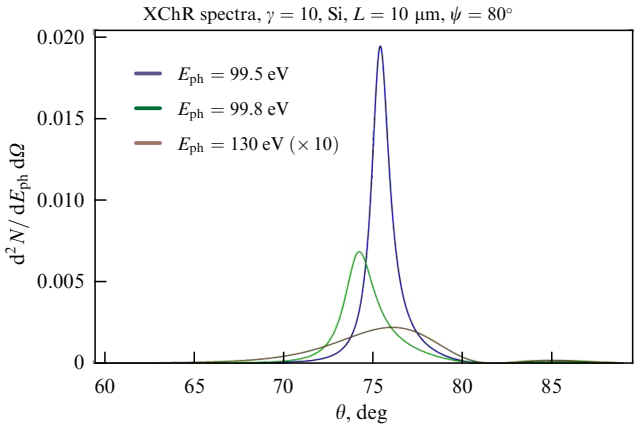

Figure 5. Same as Fig. 4 for $\psi = 80°$.

In the X-ray range, the dependence of this parameter on the wavelength is determined by $\chi'(\omega)$. As the tilt angle ψ increases, the asymmetry of the VCR cone increases: the photon yield at an angle $\theta^0_{ch} < \psi$ increases, while for $\theta^0_{ch} > \psi$, it is suppressed (Fig. 5). Note also that for a geometry close to the grazing incidence, only a portion of the VCR cone at angles $\theta < \psi$ escapes into the vacuum, while emission at larger angles ($\theta > \psi$) is almost completely suppressed.

The increase in the intensity and asymmetry of the VCR cone with increasing tilt angle ψ is illustrated in Fig. 6a. As can be seen from the figure, for a radiator orientation of $\psi = 80°$, the right peak is absent.

Figure 6b shows the dependences of the maximum VCR intensity $d^2W/d\hbar\omega\,d\Omega$ for an energy of $\hbar\omega = 99.5$ eV for both maxima with increasing radiator tilt angle. The figure shows that, as the grazing incidence geometry is approached, the VCR yield at the 'left' maximum increases more than threefold compared to the perpendicular incidence. A similar effect was discussed in [27, 28], but the authors only reported estimates. In [29], the authors also used a polarization current model to calculate the VCR and TR characteristics in the energy range $\hbar\omega \sim 450$ eV; however, they did not obtain such a sharp dependence of the VCR yield on the radiator tilt angle, possibly due to the smallness of the angle $\theta^0_{ch}(\sqrt{\chi'(450\text{ eV}) - \gamma^{-2}} \approx 4.3°)$.

6. Spectral distribution of Vavilov–Cherenkov radiation

The spectral and angular distribution of the VCR photon yield $d^2N/\hbar\,d\omega\,d\Omega$ is calculated using the well-known formula

$$\frac{d^2N}{\hbar\,d\omega\,d\Omega} = \frac{1}{\hbar\omega}\,\frac{d^2W}{\hbar\,d\omega\,d\Omega}\,, \tag{46}$$

where $d^2W/\hbar\,d\omega\,d\Omega$ is determined by Eqn (14).

Figure 7a shows the photon spectra for perpendicular electron flight with $\gamma = 10$ through an Si radiator for photon emission angles near $\theta^0_{ch} = 7.2°$. It should be noted that the observation angle $\theta = 6°$ approximately corresponds to the maximum in the TR angular distribution ($\theta = 1/\gamma$), but for moderately relativistic electrons ($\gamma = 10$), the VCR contribution dominates. Figure 7b shows similar dependences for a radiator orientation of $\psi = 70°$.

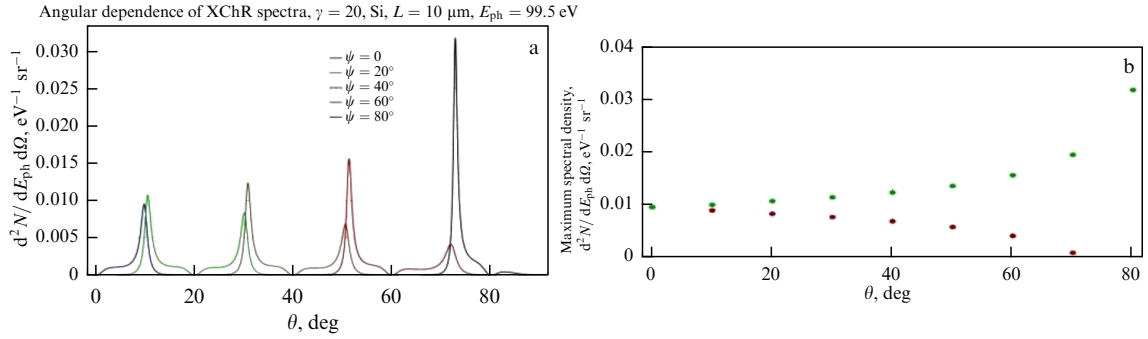

Figure 6. (a) Evolution of angular distribution of VCR with $\hbar\omega = 99.5$ eV as inclination angle ψ changes (from 0° to 80°). (b) Change in VCR intensity at maximum with increasing inclination angle (green dots — left peak, red dots — right peak).

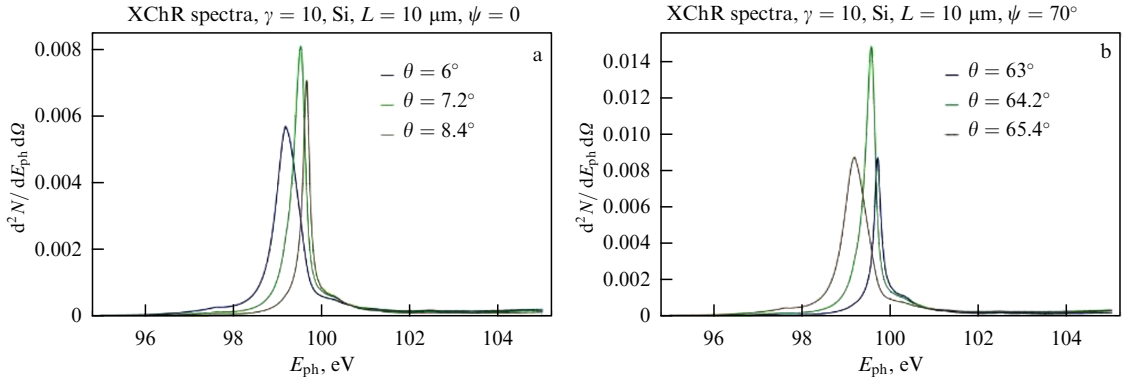

Figure 7. (a) Photon spectra for perpendicular passage of electrons with $\gamma = 10$. (b) Similar dependences for radiator orientation $\psi = 70°$.

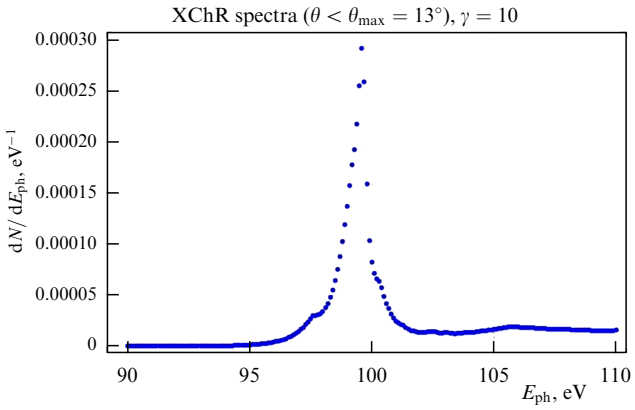

Figure 8. Spectral distribution of VCR emitted into cone with $\theta_{max} = 13°$ by electrons with $\gamma = 10$ for perpendicular geometry.

The polarization current method used in this study allows one to find the number of photons in the Cherenkov radiation cone for any radiator orientation. As the tilt angle ψ increases, the cone opening angle θ_{max} decreases (Fig. 6a). It should be noted that, in the frequency range under consideration, the term 'VCR cone' refers to a cone almost completely filled with radiation ($\theta \leqslant \theta_{max}$, $\theta_{max} > \theta_{ch}^0$). In the optical range, the VCR cone [30] refers to the space bounded by two conical surfaces with opening angles

$$\theta_{1,2} = \theta_{ch} \pm \Delta\theta = \theta_{ch} \pm \frac{2\lambda}{\pi L}\frac{\sin\theta_{ch}}{\cos\theta_{ch}}\,.$$

Figure 3a shows the angular distribution of VCR from a silicon target for a perpendicular flight. The photon spectrum is obtained by calculating the integral

$$\frac{dN}{d\hbar\omega} = 2\pi\int_0^{\theta_{max}} \frac{d^2N}{d\hbar\omega\,d\Omega}\sin\theta\,d\theta\,, \tag{47}$$

where $\theta_{max} \approx 13°$ (Fig. 3a).

Figure 8 shows the spectral distribution of VCR into a cone with an opening angle $\theta_{max} = 13°$.

The number of photons emitted into this cone is determined by the expression

$$\Delta N = \int_{\hbar\omega_{min}}^{\hbar\omega_{max}} d\hbar\omega\,\frac{dN}{d\hbar\omega}\,. \tag{48}$$

The VCR spectrum of electrons with $\gamma = 10$ in the full cone remains monochromatic (see Fig. 8), but the 'trace' of the VCR cone on the detector located at a distance $D = 500$ mm from the radiator is a ring of radius $R = D\sin 7.2° = 62.5$ mm and a width of ~ 3.5 mm.

In the case under consideration, the photon yield $\Delta N = 0.00037$ photons/electron.

It is of interest to estimate the photon yield and the VCR spectral linewidth when forming a photon beam with a collimator with a given aperture, located at a distance D at an angle $\theta_D \approx \psi - \theta_{ch}^0$. In the simplest case of a square aperture with side a, the emission spectrum is determined by integrating Eqn (14) over the solid angle $d\Omega = \sin\theta\,d\theta\,d\varphi$.

In experiments, the condition

$$\frac{a}{D} \ll 1 \tag{49}$$

is usually satisfied. The calculation results for a square aperture with dimensions $a = 2$ cm, located at a distance of $D = 50$ cm, are presented below.

To obtain the spectrum of a collimated VCR, it is necessary to calculate the integral

$$\frac{dN}{\hbar\,d\omega} = 2\int_0^{\varphi_{max}} d\varphi\int_{\theta_{min}}^{\theta_{max}} \sin\theta\,d\theta\,\frac{d^2N}{\hbar\,d\omega\,d\Omega}\,,$$

$$\varphi_{max} = \frac{a}{2D}\sin\theta_D\,, \tag{50}$$

$$\theta_{min} = \theta_D - \frac{a}{2D}\,,$$

$$\theta_{max} = \theta_D + \frac{a}{2D}\,.$$

Figure 9 shows the spectral line shape of a collimated VCR for perpendicular geometry and an observation angle of $\theta_D = 1/\gamma = 5.7°$ ($\gamma = 10$, as in the previous examples).

As noted above, for moderately relativistic electrons, the contribution of TR to the resulting photon yield is negligible, and the emission spectrum at an angle of $\theta_D = 1/\gamma$ exhibits a maximum corresponding to VCR rather than a monotonically decreasing spectrum typical of TR. This type of emission is called 'hybrid' in [29].

For collimated radiation, when only a portion of the radiation near the angle θ_D is cut out from the VCR cone by a collimator with an opening $\Delta\theta \approx a/D$, $\Delta\varphi \approx a/D\sin\theta_D$, the monochromaticity of which can be determined by the spectral line width at half maximum. For the VCR line shown, this

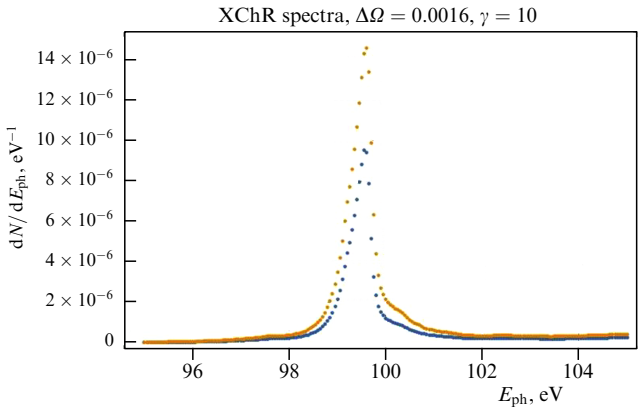

Figure 9. Spectra of collimated VCR radiation for observation angles of $\theta_D = 7.2°$ (blue dots) and $\theta_D = 5.7°$ (yellow dots).

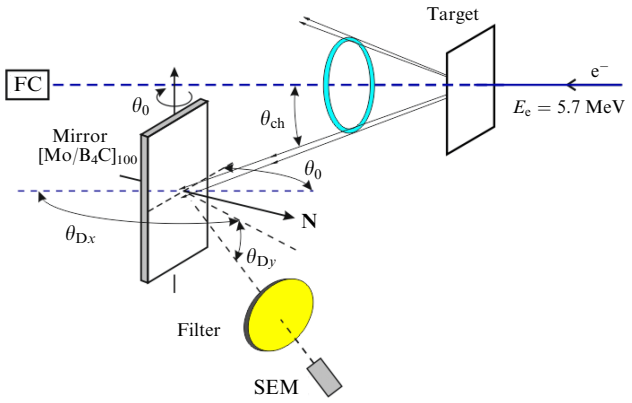

Figure 10. Experimental setup. FC is Faraday cup.

value is (at $\theta_D = 7.2°$)

$$\Delta\hbar\omega = \text{FWHM} = 0.48 \text{ eV}.$$

Apparently, the perpendicular geometry is the least favorable. The photon yield increases significantly with radiator rotation (see Fig. 6). In Section 8, the so-called grazing-incidence geometry is considered.

7. Measurement of Vavilov–Cherenkov radiation spectrum from Be and Si radiators

As noted above, when VCR is generated in the soft X-ray range by moderately relativistic electrons, the contribution of transition radiation to the spectral-angular distribution of the radiation is virtually absent.

The spectral composition of Vavilov–Cherenkov radiation from Be and Si radiators was experimentally studied using the 5.7-MeV electron beam of the Tomsk Polytechnic University microtron [31]. The experimental setup is shown in Fig. 10. A collimated electron beam (transverse size, 2.5 mm, divergence, 10^{-4} rad) with a macropulse repetition rate of 50 Hz (macropulse duration, 0.5 μs) passed through the radiator and entered the Faraday cup. The average number of electrons in a macropulse was 2.5×10^7. Be (20×20 mm) and Si (6×8 mm) samples with a thickness of 26 μm and 4 μm, respectively, were used as radiators. In both cases, the radiator thickness was much greater than the absorption length of the radiation in the target material in the photon energy range studied. A multilayer X-ray mirror [32] based on $[Mo/B_4C]_{100}$ was used to measure the emission spectrum. It was placed 200 mm from the radiator. To eliminate the generation of radiation by electrons scattered by the collimator, the upper edge of the mirror was located 20 mm below the beam trajectory.

The working size of the mirror was formed by a rectangular vertical Mylar diaphragm measuring 10×35 mm^2. The mirror consists of 100 pairs of Mo and B_4C layers located on a silicon substrate. The mirror period is 7.56 nm, and the ratio of the B_4C layer thickness to the period is 0.5. The composition of the transition layers was estimated as a mixture of $^5Mo + B_4C$ with a thickness of 0.9–0.95 nm. The reflectivity of the mirror, calculated in the IMD-5 package [33] in the specular scattering approximation, was 30–35% in the photon energy range $\Delta E = 80 - 120$ eV.

A spiral channel electron multiplier (CEM) with a bell (model VEU-6) [34] was used as a detector of the reflected radiation from the mirror, located at a distance of 144 mm from the mirror. The channel electron multiplier operated in counting mode, maintaining linearity with a loading of up to 2 pulses per macropulse. The VEU-6 loading rate, which was monitored for every 100 accelerator ejection events, was 10–20 pulses for every 100 ejections. The detector detection efficiency, averaged over the entrance window with a diameter of 9 mm, was 6.9% at a photon energy of 96.7 eV and 6.5% at a photon energy of 77.1 eV. The lower energy threshold of photon registration was 12 eV [35–37]. The distance from the multilayer mirror to the SEM was 144 mm. A block of permanent rare-earth magnets was installed between the detector and the mirror to protect the detector from scattered electrons as was a plastic filter made of nitrocellulose with a thickness of 0.2 μm. This filter allowed suppression of the soft part of the background radiation ($E < 50$ eV). The block was placed inside a steel housing with a through hole with a diameter of 15 mm, which acted as a preliminary collimator. Two additional slits with widths of 7 and 8 mm were installed inside the steel housing in the center and at the exit to shape the beam of registered radiation. Thus, the optical axis of the radiation detection system between the mirror and the detector was formed by diaphragms in the direction of specular reflection of a portion of the Vavilov–Cherenkov radiation cone corresponding to $\theta_{ch} = 6.5°$ ($\theta_{Dy} = 6.5°$, see Fig. 10). The angular dimensions and solid angle of the detected radiation were $\Delta\theta_{ch}^x = \pm 0.67°$, $\theta_{ch}^y = \pm 0.74°$ and $\Omega = 6 \times 10^{-4}$ sr, respectively. The axis of rotation of the detecting system coincided with that of the multilayer mirror.

In the experiment, for each value of angle θ_0, the intensity of the radiation reflected from the multilayer mirror in the Bragg direction was determined from measurements of the dependence of the radiation intensity on the observation angle θ_{Dx} with the corresponding movement of the detector (see Fig. 10).

The maximum values in the angular distribution of the radiation intensity after background subtraction were used to plot the radiation intensity as a function of the orientation angle of the multilayer mirror θ_0.

The calculated intensity of radiation from Be and Si radiators, reflected by a multilayer mirror in the Bragg direction, as a function of the mirror orientation angle θ_0 is shown in Fig. 11.

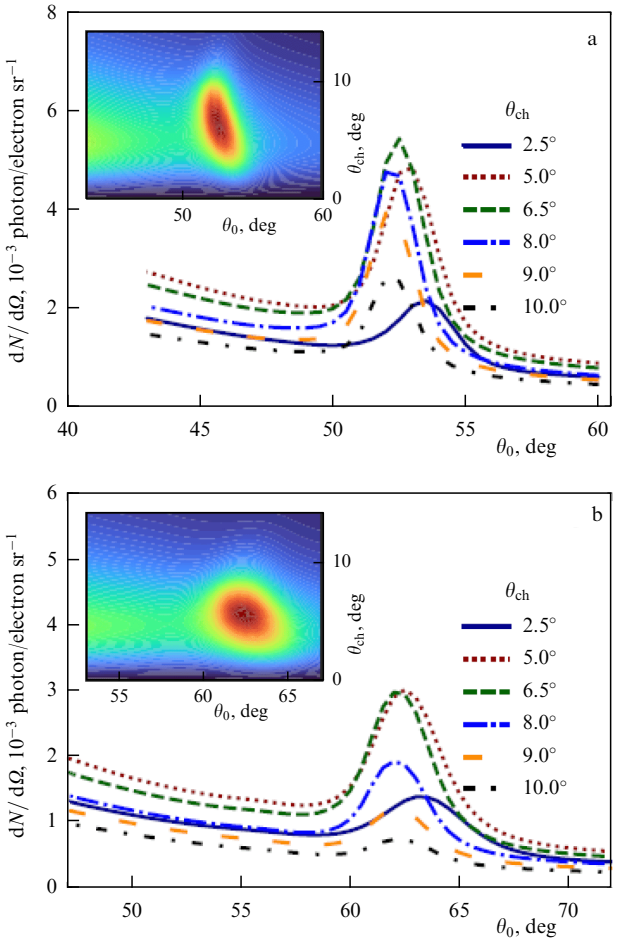

Figure 11. Calculated intensity of radiation reflected by $[Mo/B_4C]_{100}$ multilayer mirror as a function of mirror orientation angle θ_0 for Be (a) and Si (b) targets.

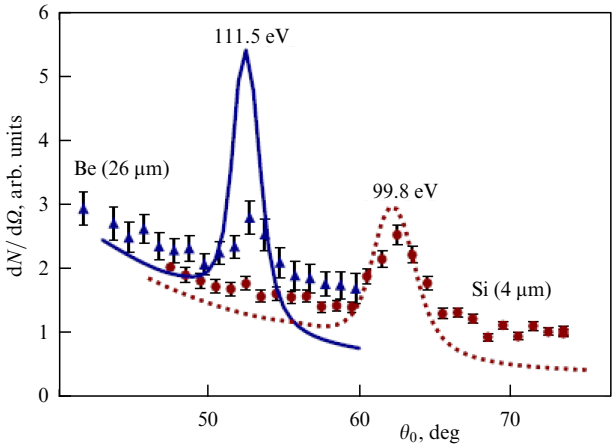

Figure 12. Intensity of radiation reflected by multilayer mirror as function of mirror tilt angle θ_0 for Be and Si radiators. Curves — theoretical calculation; dots — experimental data.

Calculations made for VCR emitted at various angles θ_{ch} took into account the electron energy and the reflectivity of the multilayer mirror, calculated using the recurrence relations method [38–40], for transition and Cherenkov radiation photons in the spectral range $\Delta E = 30-400$ eV. Since the maximum intensity of Vavilov–Cherenkov radiation from both Be and Si radiators corresponds to an observation angle $\theta_{ch} = 6.5°$, the measurements were carried out for this angle.

Figure 12 presents the measured and calculated intensity of radiation reflected by a multilayer mirror as a function of the mirror tilt angle θ_0 for Be and Si radiators. The calculation was carried out for the case of an ideal multilayer mirror. The behavior of the measured dependences and the positions of the maximum values are in good agreement with the calculated results. The maximum intensities at angles $\theta_0 = 62°$ and $\theta_0 = 52°$ correspond to energies $E_{Si} = 99.8$ eV and $E_{Be} = 111.5$ eV.

The values of E_{Si} and E_{Be} are in good agreement with the L and K absorption edges of silicon and beryllium, respectively. Thus, it can be concluded that Vavilov–Cherenkov X-rays are detected from Be and Si radiators.

It should be noted that a detailed comparison of the results reveals some disagreements between the experimental data and the calculated ones in the peak region, including the presence of a background pedestal. It can be assumed that the disagreement between the theoretical calculations and the measured results is due to the oxide layer and the presence of impurities on the radiator surface. The oxide layer can affect the radiation generation process in different ways: first, Cherenkov radiation will be absorbed by the oxide layer; second, the intensity of the transition radiation will depend on the permittivity of the oxide layer.

The influence of the oxide layer on the calculated radiation characteristics was taken into account using V.E. Pafomov's model [13] for the spectral-angular distribution of radiation intensity of a charge passing through a target consisting of three layers. This stage of the calculations was made for a homogeneous layer of BeO or SiO_2 oxides as an additional layer on the target surface. The calculations for BeO took into account the chemical shift, which leads to a 2.8-eV shift in the absorption edge of beryllium in combination with oxygen toward higher energies [41–43]. The chemical shift of the absorption edge in SiO_2 is 4.5 eV.

Estimates showed that the radiation intensity of the background pedestal is much higher than the contribution of bremsstrahlung. The most plausible explanation for the pedestal is the presence of holes in the plastic filter. In this case, the high intensity of the pedestal is due to the contribution from the normal reflection of the soft part of the transition radiation spectrum ($E < 60$ eV) transmitted through the holes in the plastic filter. To 'cut off' this background, the VCR spectra of Be and Si were calculated for a threshold photon energy of $E = 12$ eV, which was taken as the lower threshold of detector efficiency.

Figure 13 compares the experimental data with the calculated results obtained for a multilayer radiator, taking into account the detector efficiency, the transparency of the plastic filter, the efficiency of radiation reflection by the mirror, and the thickness of the oxide film. Good agreement between the calculated and experimental results was achieved by adjusting the oxide layer thickness and the fraction of radiation transmitted through the holes. The calculated results, shown by solid lines, were obtained with an oxide layer thickness of 180 nm and 70 nm for Be and Si, respectively, taking into account that the total aperture of the holes in the plastic filter was 1.5% of the total detector aperture. The dashed curve in Fig. 13 shows the contribution associated with the radiation transmitted through the holes in the plastic filter.

As shown in [44], the wavelength of the spectral line reflected by a multilayer X-ray mirror is calculated using the

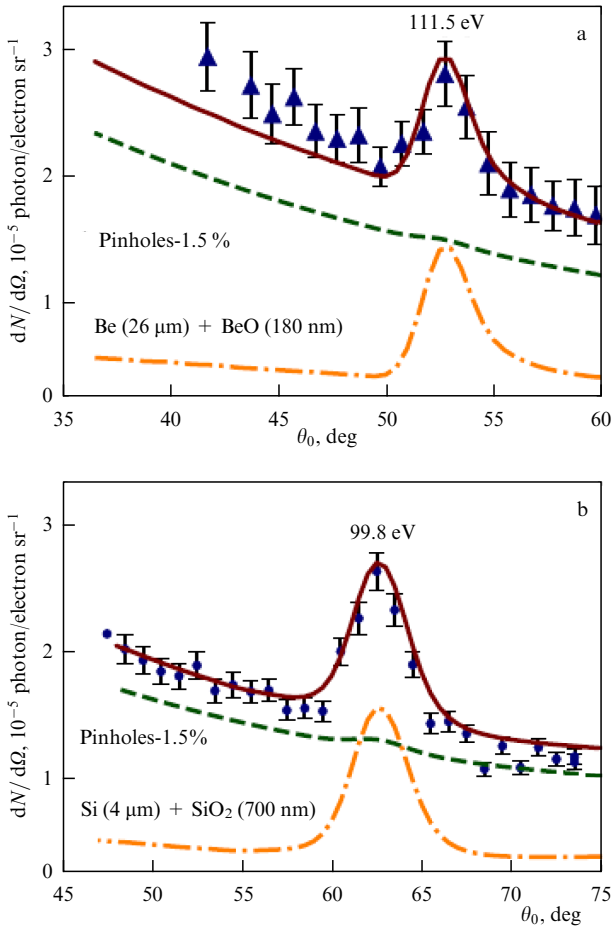

Figure 13. Comparison of calculations and experimental results.

modified Wulff–Bragg formula:

$$m\lambda = 2d\sin\theta\sqrt{1-\frac{2\overline{\delta}-\overline{\delta}^2}{\sin^2\theta}}, \qquad (51)$$

where m is the diffraction order, d is the period of the structure, and θ is the angle of incidence. The average refractive index for a multilayer mirror is

$$\mathrm{Re}\,\overline{n} = 1-\overline{\delta}, \quad \overline{\delta} = \frac{t_A\delta_A + t_B\delta_B}{t_A + t_B},$$

where t_A, t_B is the thickness of layers of material A, B; $\delta_{A,B} = 1 - \mathrm{Re}\,n_{A,B}$; $n_{A,B}$ is the refractive index in layer A, B.

Knowing the angular width of the orientation dependence of the scattered photon yield (see Fig. 13), we can estimate the monochromaticity of the radiation beam reflected by the mirror. Using Eqn (51), we obtain

$$\Delta\lambda = \frac{2d\cos\theta}{m}\sqrt{1-\frac{(2\overline{\delta}-\overline{\delta}^2)}{\sin^2\theta}} \times\left\{1+\frac{2\overline{\delta}-\overline{\delta}^2}{\sin^2\theta}-\frac{(2\overline{\delta}-\overline{\delta}^2)^2}{\sin^4\theta}\right\}. \qquad (52)$$

Disregarding the last terms in curly brackets (in our case, $\sin\theta \gg \overline{\delta}$), we obtain

$$\frac{\Delta E_{ph}}{E_{ph}} = \frac{\Delta\lambda}{\lambda} \approx \coth\theta\Delta\theta.$$

Table 1. Characteristics of VCR spectral lines in Be and Si radiators ($\gamma = 10$).

	θ	E_{ph}	$\Delta\theta$	$\Delta E_{ph}/E_{ph}$
Be	52°	111.5 eV	3°	0.04
Si	62°	99.8 eV	4°	0.03

Selecting the FWHM of the measured orientation dependence as $\Delta\theta$, we obtain the result shown in Table 1.

The monochromaticity of the reflected beam is somewhat worse than that of the initial beam ($\Delta E_{ph}/E_{ph} \sim 0.01$) due to the finite number of mirror layers and structural imperfections, but remains quite high.

8. Vavilov–Cherenkov radiation in grazing incidence geometry

The authors of [27] considered grazing incidence geometry, i.e., one in which the asymmetric VCR cone 'degenerates' into a single maximum. In our notation, the evaluation criterion for grazing incidence angles proposed in [27] is represented as

$$\frac{\pi}{2} - \left(\sqrt{\chi'} + \sqrt{\chi' - \gamma^{-2}}\right) \leqslant \psi_{gr}. \qquad (53)$$

For a silicon radiator ($\chi' \approx 0.036$) and $\gamma = 10$, from Eqn (53), we have $\psi_{gr} \geqslant 74°$, as shown in Fig. 6a, for a radiator tilt angle of $\psi = 80°$; the second maximum for $\theta > \psi$ is almost completely suppressed.

In approximation $(\pi/2 - \psi_{gr}) \ll 1$, the authors of [28] calculated the VCR intensity spectrum for a collimation of $\Delta\theta = 0.3\sqrt{\chi'}$ and showed that the photon yield for a beryllium target with a radiator orientation of $\psi = 89.4°$ (in our notation) is an order of magnitude higher than the photon yield for an angle of $\psi = 26°$.

The grazing-incidence geometry was examined in experiment [11], in which the VCR photon yield from a silicon target was measured. The experiment was conducted for radiator tilt angles of $\psi = 78°$, 84°, and 87° and for perpendicular geometry on an electron beam with an energy of 75 MeV ($\gamma = 150$). A proportional counter with a resolution of $\sim 50\%$ near the VCR line with $\hbar\omega \approx 100$ eV, movable relative to the electron beam, was used as a detector, which made it possible to measure the angular distribution of the VCR. A detector with a horizontal aperture of 6.4 mm, located 75 cm from the radiator, provided a polar angle 'capture' of $\Delta\theta = \pm 4.5$ mrad, while the vertical aperture was 1.6 mm.

Figure 14 shows the VCR photon spectra for electrons with a Lorentz factor of $\gamma = 150$ from a silicon radiator for tilt angles of $\psi = 78°$, 84°, and 87°.

In all cases, a minimum was observed in the orientation dependences when the detector was positioned on the axis of the electron beam deflected by the magnet, and symmetrical maxima near observation angles of $\theta_D = \pm 7$ mrad, which correspond to the TR mechanism. For the perpendicular geometry, in addition to these maxima, no other features were observed in the studied range of angles ($-0.06 \leqslant \theta_D \leqslant 0.06$), but for the grazing-incidence geometry, for all orientation angles ($\psi = 78°$, 84°, 87°), symmetrical maxima were observed in the angular distributions for angles $\theta_D^{exp} \approx \pm 0.04$. Estimate (26) for silicon yields a value of $\theta_D \approx 0.18 \gg \theta_D^{exp}$.

The authors suggested that the observed maxima are due to the VCR mechanism and explained this disagreement by the fact that, when averaging over the energy

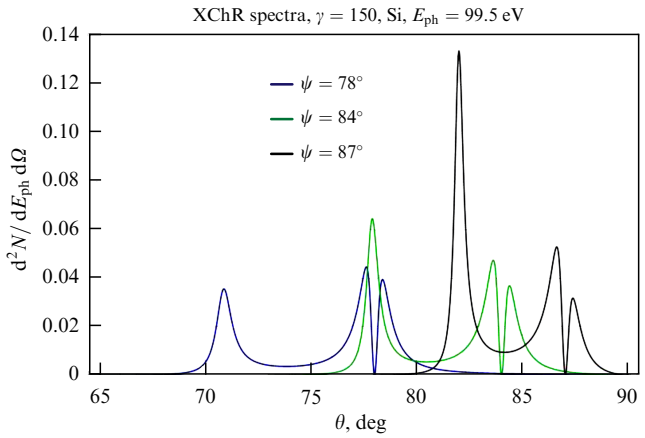

Figure 14. Increase in VCR spectral density at various tilt angles in grazing incidence geometry.

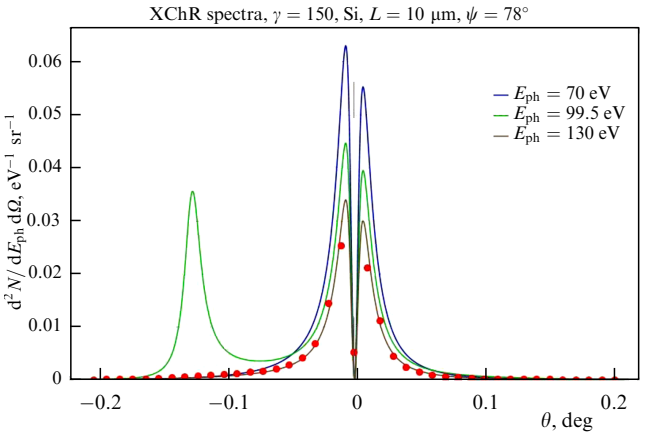

Figure 15. Results of simulation of experiment [11] (red dots) in comparison with calculated angular dependences of VCR photon yields ($\hbar\omega = 99.5$ eV — green line) and TR ($\hbar\omega = 70$ eV — blue line, $\hbar\omega = 130$ eV — brown line).

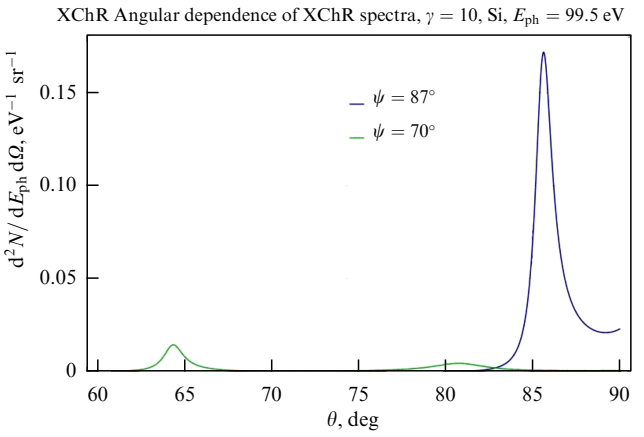

Figure 16. Spectral-angular distribution of VCR photon yield for tilt angles of silicon radiator of $\psi = 70°$ (green line) and $\psi = 87°$ (blue).

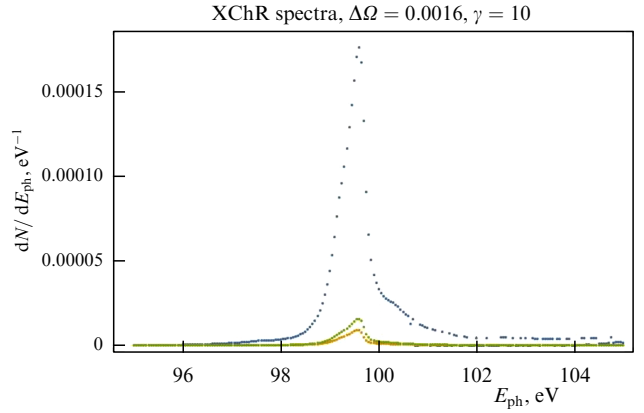

Figure 17. Spectra of collimated VCR for tilted radiator ($\psi = 70°$ — green, $\psi = 87°$ — blue) in comparison with similar spectrum for perpendicular geometry (yellow).

interval set by the energy resolution (~ 100 eV), the value of $\langle\chi'\rangle$ decreases significantly, which leads to a decrease in the angle θ_D.

The authors of the cited article hypothesized that averaging over the energy interval $\hbar\omega_{min} = \hbar\omega_{ch}(Si)(1-0.5)$, $\hbar\omega_{max} = \hbar\omega_{ch}(Si)(1+0.5)$ should narrow the Cherenkov cone severalfold.

The results of the modeling of the measured angular dependence for $\psi = 78°$, taking into account integration over the detector aperture ($\Delta\Omega = 0.000018$ sr) (see Eqn (50)) followed by integration over the spectrum (within $\hbar\omega = 70-162$ eV (see Fig. 2) of the cited article) are shown in Fig. 15 (red dots). The results were normalized to the solid angle and energy interval ($\hbar\Delta\omega = 92$ eV).

For comparison, the same figure also displays the calculated angular distributions of the VCR as a function of the angle $\theta_e = \psi - \theta$ (the angle between the electron beam axis and the detector axis).

As follows from the figure, except for the maxima in the angular range $\theta_e \sim 1/\gamma \sim 7$ mrad, no maxima due to VCR are observed.

It should be noted that the authors of [11] present the measured absolute photon yield in Fig. 2 ($\Delta N \sim 0.6$ photons/$e^- \Delta\Omega\,\Delta\hbar\omega$ for $\psi = 78°$, $\theta_e \sim 0.007$). The results of modeling for this range of angles, where the main contribution is due to the TR mechanism, yield a value of $\Delta N \sim 0.025$ photons/$e^- \Delta\Omega\,\Delta\hbar\omega$ (see Fig. 3), which is more than an order of magnitude smaller.

Apparently, the explanation for the measured yield of photons with energies of $70 < \hbar\omega < 162$ eV in experiment [11], where distinct symmetrical maxima were observed at $\theta = \pm 0.04$ for grazing incidence angles, requires a different interpretation.

It is of interest to determine the potential of employing grazing-incidence geometry for moderately relativistic electron energies ($\gamma = 10$) using PCM. Figure 16 shows the angular dependences of the VCR photon yield with energy $\hbar\omega = 99.5$ eV for silicon radiator tilt angles of $\psi = 70°$ (outside grazing-incidence geometry) and $\psi = 87°$. In the latter case, the spectral-angular distribution of the VCR is approximately an order of magnitude greater than the similar characteristic for $\psi = 70°$.

Figure 17 shows the collimated emission spectra for various tilt angles $\psi = 0$ ($\theta_D = 7.2°$); $\psi = 70°$ ($\theta_D = 64.2°$); $\psi = 87°$ ($\theta_D = 85.6°$).

Calculations were carried out using Eqn (50) for a square aperture ($a = 2$ cm) of the detector, located at an angle θ_D at a distance of 50 cm from the radiator.

Data displayed in Table 2 illustrates the VCR spectral line characteristics for various radiator tilt angles.

Table 2. Characteristics of VCR spectral lines in silicon radiator ($\gamma = 10$).

ψ	$\Delta\hbar\omega$, eV	Monochromaticity, %	ΔN, photon/e$^-$
0	0.48	0.48	6.3×10^{-6}
70°	0.53	0.53	10.3×10^{-6}
87°	0.57	0.57	128×10^{-6}

In [28], the authors predicted that, for tilt angles close to 90° (see Eqn (51)), the VCR photon yield increases by an order of magnitude compared to the perpendicular geometry.

The results presented in Table 2 confirm this conclusion (the excess photon yield for the grazing geometry reaches ~ 20). The spectral linewidth increases only slightly.

Unfortunately, experimental studies of the VCR for the grazing geometry (except for an earlier experiment [11]) are lacking.

9. Conclusions

Equations (14) obtained in the PCM for the spectral-angular distribution of the radiation intensity of a charge passing through a radiator with permittivity $\varepsilon(\omega)$ adequately describe the characteristics of X-ray emission (including in the region of anomalous dispersion) for arbitrary radiator orientation. For a perpendicular charge flight, the PCM yields results that agree within a few percent with a model based on the small-angle approximation of transition radiation theory [5, 6, 10]. For a large mismatch of orientation angles close to the grazing incidence geometry, the results obtained using the PCM without resorting to the small-angle approximation are generally consistent with the results published in [29]. The calculation results show a noticeable increase in the X-ray VCR intensity for orientation angles satisfying condition (53).

W. Knulst, in his dissertation [12], estimated the photon yield of monochromatic radiation for various materials and found a correlation between the value of χ' and the number of photons ΔN. For example, it follows from the results reported in [45] that $\Delta N(\mathrm{Si}) = 1.7 \times 10^{-3}$ and $\Delta N(\mathrm{Ti}) = 2.4 \times 10^{-4}$, since the corresponding susceptibilities differ by approximately an order of magnitude: $\chi'(\mathrm{Si}) = 4 \times 10^{-2}$, $\chi'(\mathrm{Ti}) = 7 \times 10^{-3}$.

As noted earlier, for a geometry close to the grazing incidence, the spectral-angular radiation density increases significantly. By placing the collimator at the required angle, one can expect the photon yield to be enhanced.

It is of interest to find the spectral line intensity (the number of photons per initial electron) for a titanium radiator in the VCR photon energy region of approximately 450 eV using the PCM and compare it with estimates presented in [6, 7]. By interpolating the tabular data from [20] and calculating the plasma frequency [4]

$$\omega_\mathrm{p} = 21\sqrt{\frac{2Z}{A}\rho}\,, \tag{54}$$

where Z is the atomic number of the radiator material, A is its atomic weight, ρ is its density, we can find the functions χ' and χ'' for Ti at $\omega_\mathrm{p} = 42.8$ (Fig. 18).

Figure 19a shows the angular distributions of the photon yield with energies near $\hbar\omega = 452$ eV, from which an angle of $\theta_\mathrm{D} = 85.2°$ can be selected for the collimator placement. The spectra of collimated radiation ($a = 2$ cm, $D = 50$ cm) for electrons with energies of $E_\mathrm{e} = 10$ MeV for various radiator orientations ($\psi = 0$, $\psi = 87°$) are presented in Fig. 19b. The same figure shows the spectrum of radiation in a full cone ($\theta_\mathrm{max} = 6°$).

Table 3 presents the characteristics of the VCR spectral lines from a titanium radiator.

The photon yield in a full cone ($\theta < \theta_\mathrm{max} = 6°$) virtually coincides with Knulst's estimate, whereas, for an Si radiator, the same quantity (for $\theta < 13°$), albeit exceeding the photon yield for Ti ($\Delta N = 0.00037$), is significantly lower than Knulst's estimate [12].

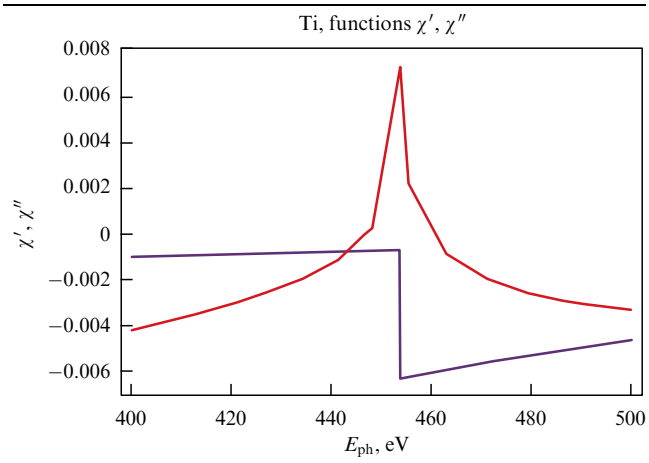

Figure 18. Functions χ' (red line) and χ'' (blue) characterizing the permittivity of titanium.

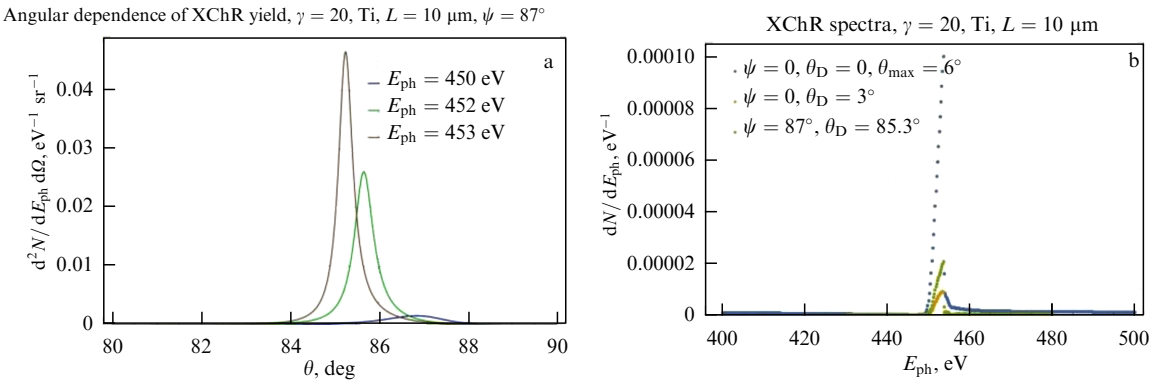

Figure 19. (a) Angular distribution of photon yield of different energies from titanium radiator in grazing incidence geometry, (b) VCR spectrum in 'full' cone ($\theta_\mathrm{max} = 6°$) for perpendicular geometry (blue dots) and spectral lines of collimated radiation ($\Delta\Omega = 0.0016$). Yellow dots — perpendicular geometry, green — grazing incidence geometry ($\psi = 81°$).

Table 3. Characteristics of VCR spectral lines in titanium radiator ($\gamma = 20$).

ψ	θ_{D_1}	θ_D	$\hbar\omega$, eV	Monochromaticity, %	ΔN, photon/e$^-$
0	0	6°	1.1	0.2	0.00021
0	3°	±1.15°	1.0	0.2	0.000020
87°	85.3°	±1.15°	1.0	0.2	0.000042

It should be noted that, for a Ti radiator, the photon yield for the grazing incidence geometry increases, but not as much as for an Si radiator.

The authors of [29] also used the PCM to calculate the VCR characteristics of a titanium radiator; however, the calculations were made for an angle ψ, for which no noticeable increase in photon yield was observed (due to the fact that, for Ti, according to criterion (53), the onset of the grazing incidence geometry occurs at an angle $\psi = 81°$). If we consider the intensity of collimated radiation, then, by comparing the data in Tables 2 and 3 for the perpendicular flight, we can conclude that the correlation proposed by Knulst is completely absent and only manifests itself for the grazing incidence geometry.

As noted above, the PCM, considering the VCR and TR processes as a manifestation of the same polarization radiation mechanism, describes the VCR and TR characteristics using a universal expression (14), valid for arbitrary radiator orientation, in contrast to the approach of [1, 5]. The considered characteristics of the radiation of moderately relativistic electrons exhibit features of both VCR and TR, since the cones of both types of radiation overlap to a significant extent (hybrid radiation). However, as the electron energy increases, the cones 'separate,' making it possible to isolate the VCR mechanism and suppress the contribution of TR by means of angular selection

The above examples of theoretical calculations and measurement results show that the spectral and angular characteristics of the Vavilov–Cherenkov X-ray radiation of moderately relativistic electrons is primarily determined by the dielectric properties of the radiator. The resonant behavior of the permittivity near the photoabsorption edge determines the monochromaticity of the radiation, while the ratio of the real part of the permittivity to the imaginary part, which characterizes the absorption properties of the radiator, determines the intensity and monochromaticity of the radiation. The results obtained are in good agreement with the criterion proposed by V.A. Bazylev for Vavilov–Cherenkov X-ray radiation [1, 5, 46]: $\mathrm{Re}\,\varepsilon - 1 > \mathrm{Im}\,\varepsilon$.

The oblique passing of a charged particle through a radiator leads to an asymmetry in the angular distribution of the radiation intensity. This angular asymmetry is due to the presence of an imaginary component of the permittivity, since increasing the orientation angle of the radiator relative to the charged particle's trajectory changes the Vavilov–Cherenkov radiation path in the absorbing medium. Thus, the effective size of the radiation source changes for different observation angles. Calculation results show a significant increase in the X-ray VCR intensity for orientation angles satisfying condition (51). Although the angle between the Vavilov–Cherenkov radiation and the electron beam remains small in the grazing-incidence geometry, the use of multilayer X-ray mirrors allows the deflection of a monochromatic X-ray beam at large angles, making it possible to use such a beam for applied purposes.

This review was prepared with the financial support of the Ministry of Science and Higher Education of the Russian Federation as part of the Tomsk Polytechnic University Development Program no. FSWW-2023-0003.

References

1. Bazylev V A et al. *Sov. Phys. JETP* **54** 884 (1981); *Zh. Eksp. Teor. Fiz.* **81** 1664 (1981)
2. Cerenkov P A *Usp. Fiz. Nauk* **93** 385 (1967); *Dokl. Akad. Nauk USSR* **2** 451 (1934); *C.R. Acad. Sci. USSR* **2** 451 (1934)
3. Tamm I E, Frank I M *Dokl. Akad. Nauk USSR* **14** 107 (1937); Frank I, Tamm I *C.R. Acad. Sci. USSR* **14** 109 (1937); Tamm I E, Frank I M *Usp. Fiz. Nauk* **93** 388 (1967)
4. Garibyan G M, Shi Ya *Rentgenovskoe Perekhodnoe Izluchenie* (X-Ray Transition Radiation) (Yerevan: Izd. AN ArmSSR, 1983)
5. Bazylev V A, Zhevago N K *Sov. Phys. Usp.* **25** 565 (1982); *Usp. Fiz. Nauk* **137** 605 (1982)
6. Knulst W et al. *Appl. Phys. Lett.* **79** 2999 (2001)
7. Knulst W et al. *Appl. Phys. Lett.* **83** 4050 (2003)
8. Gary C et al. *Nucl. Instrum. Meth. Phys. Res. B* **227** 95 (2005)
9. Uglov S et al. *Europhys. Lett.* **118** 34002 (2017)
10. Uglov S R, Vukolov A V *JINST* **16** P07043 (2021) DOI:10.1088/1748-0221/16/07/P07043
11. Moran M J et al. *Nucl. Instrum. Meth. Phys. Res. B* **48** 287 (1990)
12. Knulst W "Cherenkov radiation in the soft X-ray region: towards a compact narrowband source," PhD Thesis (Eindhoven: Thechnische Univ., 2004) DOI:10.6100/IR572080
13. Pafomov V E *Trudy Fiz. Inst. Akad. Nauk* **44** 28 (1969)
14. Karlovets D V, Potylitsyn A P "Universal description for different types of polarization radiation," arXiv:0908.2336v2
15. Shevelev M, Konkov A, Aryshev A *Phys. Rev. A* **92** 053851 (2015)
16. Potylitsyn A P, Gogolev S Yu *Phys. Part. Nucl. Lett.* **16** 127 (2019); *Pis'ma Fiz. Elem. Chast. Atom. Yad.* **16** 147 (2019)
17. Karlovets D V *J. Exp. Theor. Phys.* **113** 27 (2011); *Zh. Eksp. Teor. Fiz.* **140** 36 (2011)
18. Amus'ia M Ya et al. *Polyarizatsionnoe Tormoznoe Izluchenie Chastits i Atomov* (Polarization Bremsstrahlung of Particles and Atoms) (Exec. Eds V N Tsytovich, I M Oiringel) (Moscow: Nauka, 1987)
19. Potylitsyn A et al. *Phys. Lett. A* **417** 127680 (2021)
20. Henke B L, Gullikson E M, Davis J C *Atom. Data Nucl. Data Tables* **54** (2) 181 (1993)
21. Bolotovskii B M *Usp. Fiz. Nauk* **62** 201 (1957)
22. Grishin V M *Phys. Usp.* **65** 641 (2022); *Usp. Fiz. Nauk* **192** 689 (2022)
23. Cherry M L et al. *Phys. Rev. D* **10** 3594 (1974)
24. Bolotovskii B M *Trudy Fiz. Inst. Akad. Nauk* **140** 95 (1982)
25. Ter-Mikaelian M L *High-Energy Electromagnetic Processes in Condensed Media* (New York: Wiley-Intersci., 1972); *Vliyanie Sredy na Elektromagnitnye Protsessy pri Vysokikh Energiyakh* (Influence of the Environment on Electromagnetic Processes at High Energies) (Yerevan: Izd. AN ArmSSR, 1969)
26. Baier V N, Katkov V M *Phys. Rep.* **409** 261 (2005)
27. Kubankin A et al. *Nucl. Instrum. Meth. Phys. Res. B* **252** 124 (2006)
28. Kubankin A et al. *Radiat. Phys. Chem.* **75** 913 (2006)
29. Shevelev M V et al. *Quantum Beam Sci.* **8** (1) 6 (2024)
30. Mather R L *Phys. Rev.* **84** 181 (1951)
31. Gridnev V I et al. *Nucl. Instrum. Meth. Phys. Res. B* **28** (1) 128 (1987)
32. Innovative Technologies in X-ray Optics. Interoptics, LLC, http://www.interoptics.ru
33. XOP. X-ray Oriented Programs, http://www.esrf.eu/Instrumentation/software/data-analysis/xop2.3
34. Secondary Electron Multiplier VEU-6. Baspik, LLC, https://baspik.com/products/detectors/kanaltrony-vcu/vtorichno-elektronnyj-umnozhitel-veu-b/
35. Ainbund M R, Polenov B V *Vtorichno-Elektronnye Umnozhiteli Otkrytogo Tipa i ikh Primenenie* (Secondary Electron Multipliers of Open Type and Their Applications) (Moscow: Energoizdat, 1981)
36. Mack J E, Paresce F, Bowyer S *Appl. Opt.* **15** 861 (1976)
37. Legkodymov A A et al. *J. Surf. Investig. X-ray Synchrotron Neutron Tech.* **6** 404 (2012); *Poverkhnost'. Rentgen., Sinkhrotron. Neitron. Issled.* (5) 31 (2012)
38. Parratt L G *Phys. Rev.* **95** 359 (1954)

39. Vinogradov A V, Kozhevnikov I V *Trudy Fiz. Inst. Akad. Nauk* **196** 62 (1989)
40. Kon V G *Poverkhnost'. Rentgen., Sinkhrotron. Neitron. Issled.* (1) 23 (2003)
41. Nefedov V I *Rentgenoelektronnaya Spektroskopiya Khimicheskikh Soedinenii* (X-ray Electron Spectroscopy of Chemical Compounds) (Moscow: Khimiya, 1984) Handbook
42. Palik E D (Ed.) *Handbook of Optical Constants of Solids* Vol. 3 (San Diego, CA: Academic Press, 1998)
43. Wagner C D et al. *Handbook of X-ray Photoelectron Spectroscopy* (Eden Prairie, MN: Perkin-Elmer, 1979)
44. Coppens P et al. *Synchrotron Radiation Crystallography* (London: Academic Press, 1992)
45. Knulst W et al. *Proc. SPIE* **5196** 393 (2004)
46. Bazylev V A et al. *JETP Lett.* **24** 371 (1976); *Pis'ma Zh. Eksp. Teor. Fiz.* **24** 406 (1976)